TUDelft

Delft University of Technology

Numerical Analysis of Free Flow over Rectangular Sharp-Crested Compound Weirs

Yildiz, Burhan; Uijttewaal, Wim

Important note
To cite this publication, please use the final published version (if applicable).
Please check the document version above.

Numerical Analysis of Free Flow over Rectangular Sharp-Crested Compound Weirs

Burhan Yildiz[1], Wim Uijttewaal[2]

[1] Mugla Sitki Kocman University, Mugla, Turkey, e-mail: burhanyildiz@mu.edu.tr
[1,2] Delft University of Technology, Delft, The Netherlands, e-mail: w.s.j.uijttewaal@tudelft.nl

Abstract

Compound weirs are used as flow diversion structures by adding additional flow resistance to the anticipated regions at the rivers. Furthermore, they are used for measuring and regulating flow rates accurately over a wide range of flow depths. When they are used for this purpose, the cross sections are generally selected as symmetrical having the lowest level of the weir at the middle to constrain large flow contractions. However, when used as a flow diversion structure, the cross sections should be adjusted for different degrees of flow contractions to satisfy the anticipated amount of flow resistance. The literature includes several studies in which compound weirs are modelled as flow measurement structures. Modelling them with the aim of flow diversion received little interest in literature. The adaptation of previously proposed analytical and experimental weir models has problems especially in cases with high flow contractions. In this study, the free flow over the compound weirs is modelled numerically with the application of flow diversion in mind. The results are validated by comparing them with the surface velocity measurements obtained using Surface Particle Image Velocimetry (SPIV). The study aims at understanding how far upstream flow redistribution takes place, how big the transverse mass fluxes are and how this affects the flow at the weir openings, at various degree of flow contractions. Three compound weir configurations were used: One with high flow contraction and the other two with moderate to low flow contractions. The numerical model is constructed by using a three-dimensional mesh using OpenFOAM CFD solver. A multiphase flow analysis was conducted by using Volume-of-Fluid (VOF) approach. We have applied RANS modelling with $k\text{-}\omega$ SST turbulence closure. SPIV experiments were conducted in a 3-meter-wide, 20-m-long rectangular horizontal flume at the Water Lab of Delft University of Technology. A camera was mounted over the flume to record the floating particle positions during flow. The results gave the possibility to quantify transverse distribution of mass transfer among the openings at various degrees of horizontal contractions. The initiation of streamline curvature locations at the upstream were labelled such that a comparison was achieved among the configurations. The numerical model results gave the possibility to complement experimental data regarding the effective flow sections at the weir openings. In summary, the numerical model validated by the SPIV measurements helped understanding the behaviour of flow under high horizontal contraction. However, to develop a correction methodology for high contraction for the simplified 1D weir discharge prediction models, the numerical runs should be extended for various configurations and covering the submerged weir flow as well.

Keywords: Weir; Submerged weirs; Compound weirs; Sharp-crested weirs; CFD

1. INTRODUCTION

Compound weirs have been used for flow diversion purposes when located at the floodplains of the rivers (Yildiz and Uijttewaal 2023). The adaptation of the classical one-dimensional flow rate estimation methods of sharp-crested weirs have failed to predict the flow rates for compound weirs as the latter may create highly two- and three-dimensional flows. Besides the vertical contraction provided by the uniform weirs, compound weirs also may lead to horizontal contractions at various degrees depending on the selected configurations. This means that a more comprehensive modeling approach is needed. In literature, several studies dealt with various aspects of flow over sharp-crested rectangular weirs by using Computational Fluid Dynamics (CFD) models (Qu et al 2009, Mahtabi and Arvanaghi 2018). Yildiz et al (2021) showed that the interFOAM solver of OpenFOAM was very successful in modeling flow over simply contracted rectangular sharp crested weirs when coupled with $k\text{-}\omega$ SST turbulence closure. The superiority of this turbulence model on modeling flow separation has been shown previously (Jiang et al 2018). In this study, six cases of Yildiz and Uijttewaal (2023) were modeled by using a three-dimensional approach to better understand the change of flow parameters when the weir configuration changes. Also, to observe the effect of discharge change on the flow behavior, two discharge values were tested. For better understanding of the flow, surface particle image

velocimetry (SPIV) method was used to capture surface velocities at those cases. The data gathered here was also used for validation of the numerical model. The SPIV experiments were conducted at the same flume that was used at Yildiz and Uijttewaal (2023).

METHOD

Numerical models were developed to simulate the experimental conditions of Yildiz and Uijttewaal (2023). The experiments were conducted at a 20 m long, 3 m wide horizontal flume after placing 12 gate compound weir structures at the middle of the flume covering the whole width. Compound weirs were developed as sharp crested rectangular weirs by using thin plates. 2 cm thick buttresses were used to separate each weir opening. In this study, three configurations were selected to use in the numerical models. The weir heights at each weir opening are given in Table 1. These configurations were selected among the ones creating high, moderate, and low horizontal flow contractions. Two discharge values (40 and 70 l/s) were tested to see the effect of flow rate on flow characteristics. The experiments were run to satisfy modular flow conditions at the weir with a free outlet. This satisfies supercritical flow downstream.

Table 1. Weir heights (P_i) for each weir configuration (all dimensions in cm)

Configuration	P_1	P_2	P_3	P_4	P_5	P_6	P_7	P_8	P_9	P_{10}	P_{11}	P_{12}
C4	10	15	10	15	10	15	10	15	10	15	10	15
C5	15	10	15	15	10	15	15	10	15	15	10	15
C8	20	20	20	20	20	0	0	5	10	15	20	20

Three-dimensional meshes were generated for each case. Figure 1 shows the computational mesh for configuration C4. In each of the computational runs, structured meshes with hexahedral elements were used. The meshes were refined around the weir structure. Triangles or quadrilateral elements were also allowed around the weir. Each mesh used in the study included around 130000 computational cells. Additional mesh planes were used in z-direction for better resolution of the free surface.
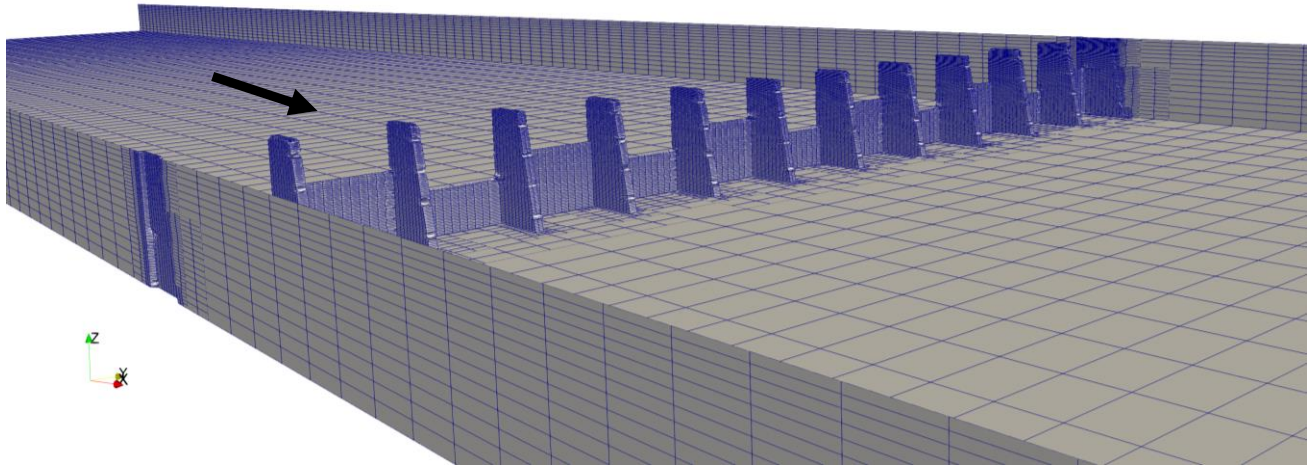

Figure 1. Computational Mesh for configuration C4 (Flow direction is indicated).

In numerical calculations, the incompressible Reynolds-Averaged Navier-Stokes (RANS) equations, which are given below, were solved.

$$\frac{\partial \overline{u_i}}{\partial x_i} = 0 \tag{1}$$

$$\frac{\partial \overline{u_i}}{\partial t} + \overline{u_j}\frac{\partial \overline{u_i}}{\partial x_j} = \overline{f_i} + \frac{1}{\rho}\left[\frac{\partial \overline{p}}{\partial x_i} + \frac{\partial}{\partial x_j}\left(\mu\frac{\partial \overline{u_i}}{\partial x_j} - \rho\overline{u_i'u_j'}\right)\right] \tag{2}$$

where, $\overline{u_i}$ is the time-averaged velocity in direction i, $\overline{f_i}$ is the time-averaged external force in direction i, $\overline{p}$ is the time-averaged pressure, ρ is density, μ is molecular viscosity, $\rho\overline{u_i'u_j'}$ is the Reynolds stress term. This

latter term was modeled by using k-ω SST turbulence model (Menter and Esch 2001, Menter et al 2003) which uses standard k-ω turbulence model at near wall zones and standard k-ε turbulence model away from the wall zones. A multiphase flow analysis was conducted to predict the interface by using the Volume-Of-Fluid (VOF) method, which defines fluid fractions at every cell and uses and additional transport equation for this parameter. The solver also includes the effect of surface tension at the interface neighboring cells. The inlet boundary condition was defined as volumetric flow rate and variable flow depth. The outlet boundary condition was defined as 'zero gradient' for velocity and pressure to ensure modular weir flow at each simulation. Side and bottom solid boundaries were selected as smooth walls with no slip conditions prevailing for velocity computations. SPIV measurements were carried out at the same horizontal flume where the research of Yildiz and Uijttewaal (2023) was carried out. A camera was mounted at the top of the flume while its camera angle was covering the whole width and extending up to 3 meters upstream of the weir. The particles were disposed at the inlet of the flume and their instantaneous positions were recorded by taking pictures. The processing of the data was done by using PIVLab tool of Matlab (Thielicke and Sonntag 2021).

RESULTS

The CFD results were first compared with the upstream flow depth (h_0) measurements of Yildiz and Uijttewaal (2023). The flow depths were measured at 5 m upstream of the weir at the experiments. The same was applied in the CFD results. The free surface levels at CFD results were estimated by interpolating for the 50% water volume fraction levels. The comparison of the CFD results with the experimental data is given in Figure 2. CFD model is successful with a maximum of 4.1 absolute percentage error deviation. It tends to underestimate the data except for the small discharge case of configuration C8. These deviations of the model results can be linked with the rather coarse mesh used in this study. The discharges measured over the weir showed up to 6% deviations from the inlet discharge. The discharge values of the numerical modeling results were estimated by integrating the velocity terms over the area below the free surface level. Therefore, it is also related with the free surface estimation method which has a dependency on mesh refinement. However, these small deviations were regarded as acceptable.
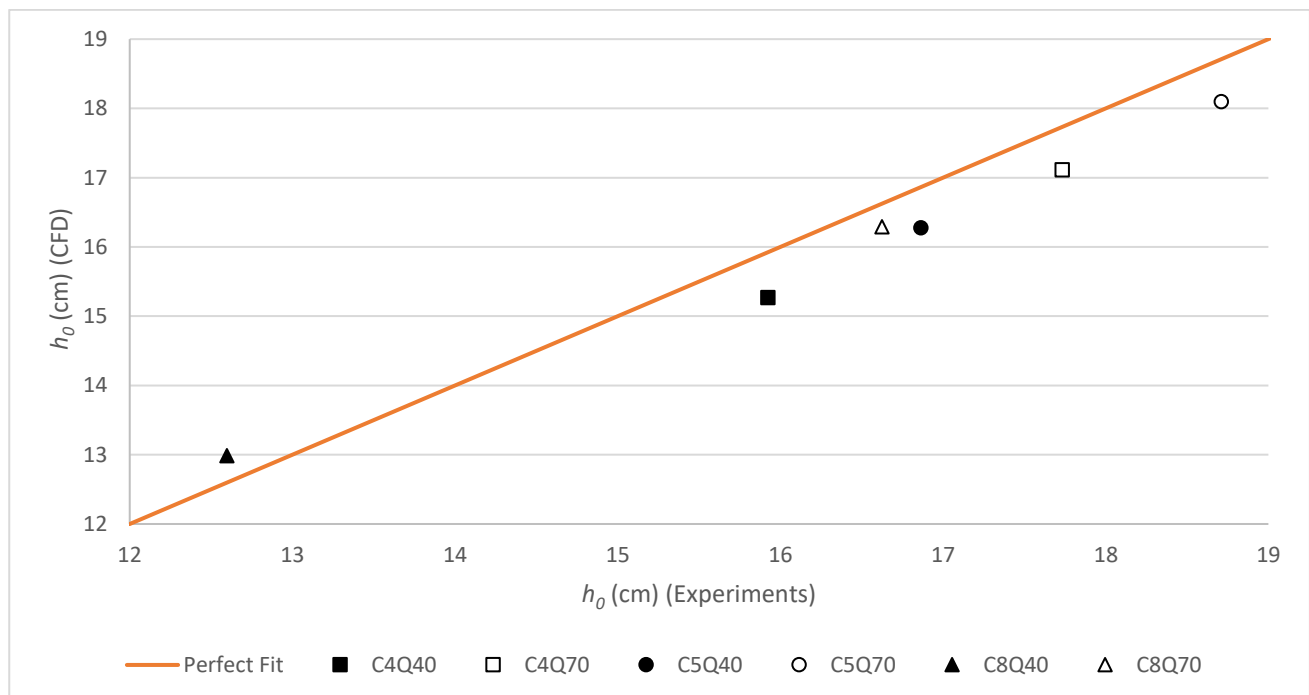

Figure 2. Comparison of measured (Yildiz and Uijttewaal 2023) and modeled upstream flow depths (h_0) at each case.

SPIV results were obtained for each case. SPIV could not capture the velocities through the whole width due to that small number of particles reached to the sides. The resolution of the particles was low or the camera could not capture them due to sinking of them as a result of high accelerations and the related surface oscillations at some regions around the weir and downstream. The comparisons of the SPIV data with the CFD results were conducted in terms of x- and y-velocity variations along some paths. The comparison

graphs are given in Figure 3. Figure 3 (a) shows comparison of streamwise velocity components (x-velocities). A path following the surface and passing through the centerline of 7th gate of the weir was taken for SPIV data. Similar methodology was applied for CFD data selecting a horizontal path 1 cm below the estimated free surface level upstream. This shift from the interface was applied to avoid possible numerical diffusions that can be observed there because of the mesh resolution. The 7th gate of weir is the one with the lowest weir height that is expected to carry the largest discharge. The weir location is at x=10 m and smaller x values correspond to the upstream from the weir. Although the maximum velocity measured by SPIV is around 0.03 m/s higher than the one that CFD provides, the comparison shows an overall good fit of the model with the measurements. This graph shows the accelerations close to the weir. The x-velocity increases to more than 4 times the approach flow velocity at the weir. The increase amount was smaller in the other configurations as expected. Figure 3 (b) shows the comparison of lateral velocity components (y-velocities) obtained from the CFD model and SPIV. A lateral horizontal path which is 25 cm upstream of the weir was selected to observe the variations in the lateral velocity component (y-velocity). Although there are some deviations at the extreme values of the velocity, the model predicts the behaviour of the change well here. The variations of y-velocities along lateral paths close to the weir is important to quantify the mass transfer through the lower weir gates and the horizontal contraction of the flow. It shows oppositely directed lateral velocities in both sides of the flume as an indicator of the mass transfer to the middle portion where lower weir gates are located. In conclusion, the assessments of the model gave confirming results and it was found successful for further application.
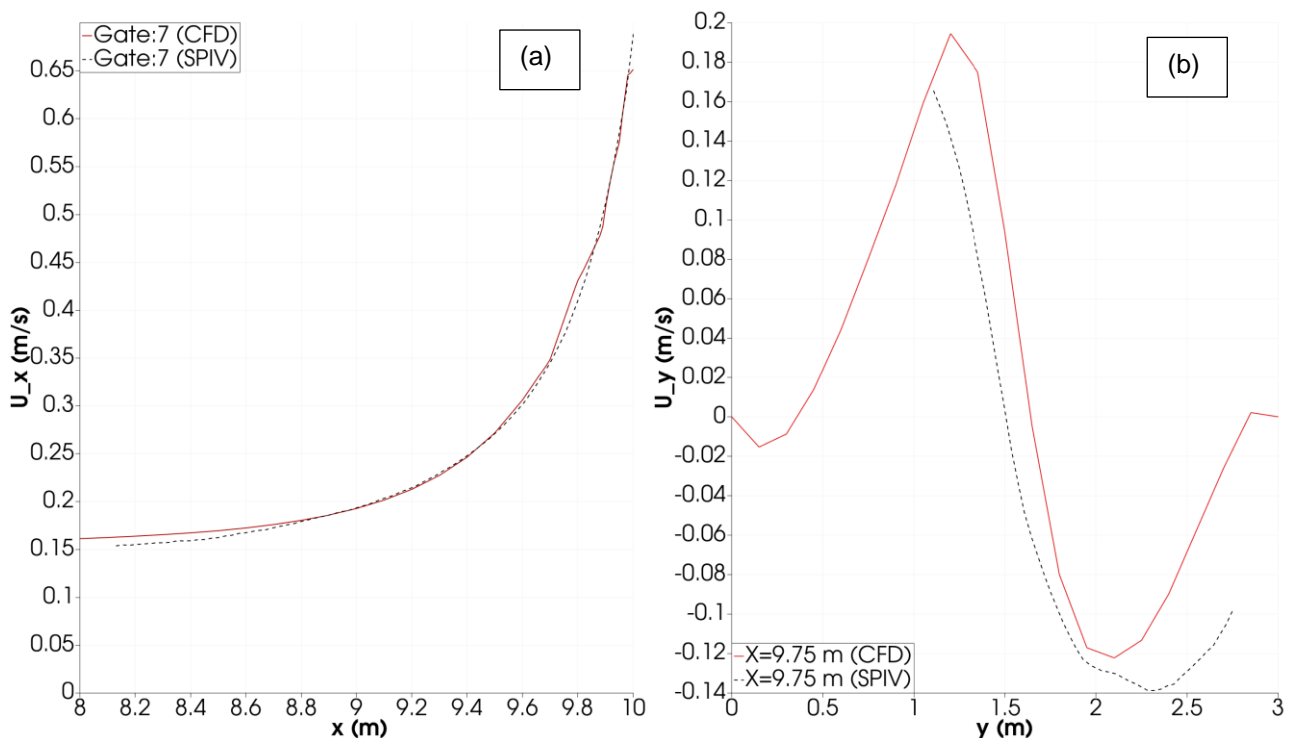

Figure 3. Comparison of SPIV and CFD results: In terms of x-velocity variations along the horizontal path extending in the streamwise direction passing through the centerline of the 7th gate of C8Q70 case on the left. In terms of y-velocity variations along the lateral path 0.25 m upstream of the weir for C8Q70 case on the right. The weir section is at x=10 m. CFD results were taken 1 cm below the free surface level.

In Figure 4, the flow depth variations over the weir are given for two cases of C8. The lowest flow depth levels were observed at Gate 6 at both discharges. The free surface level is non-symmetric there which indicates further variations of velocity within the gate section. This is validated by checking the velocity magnitude contours at the weir section for C8Q70 as given in Figure 5. The highest velocity magnitudes are observed at gate 6 owing to very large y-velocity components there. The contours are not symmetrical in the section which indicates that on the left side of the section, y-velocities are high due to the mass transfer from the further left side of the flume. Then, these velocities decrease through the right as a result of mixing with the main flow. This high lateral flow on gate 6 decreases its flow carrying capacity. The flow rate at gate 6 is smaller than the one at gate 7 although they have the same weir height.
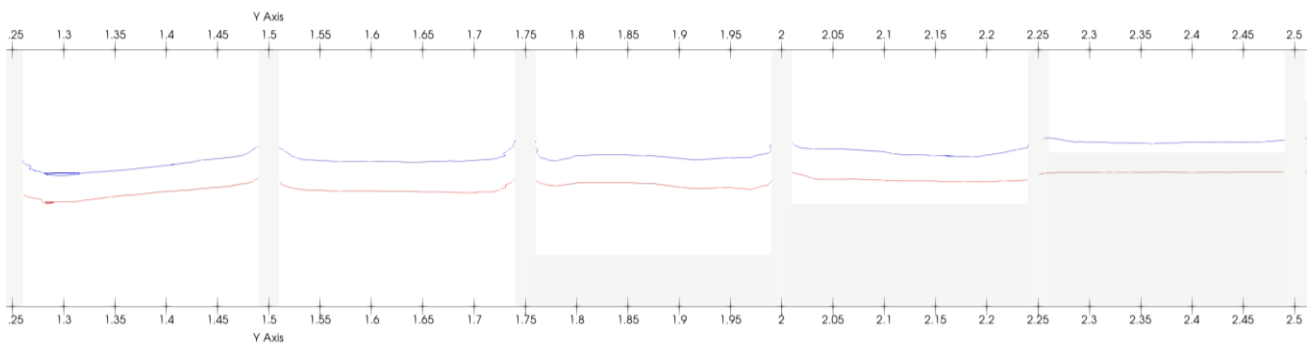
Figure 4. CFD results of flow depth levels at the weir section for C8 cases (Blue line indicates C8Q70 case, red line indicates C8Q40 case).
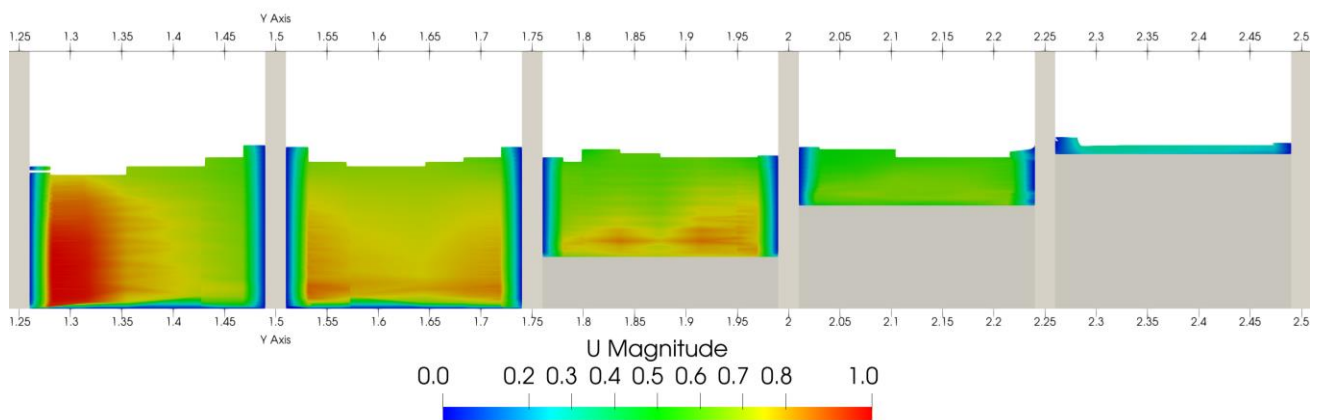

Figure 5. CFD results of velocity magnitude contours for C8Q70 case.

CONCLUSIONS

CFD models of flow over compound weirs at varying contraction rates and flow rates were accomplished. The validation of model results by using flow depth and SPIV measurements gave satisfactory outcomes with small deviations. The velocity data of the model outcome was used to identify the flow contraction. It was seen that both vertical and horizontal contractions of the flow can be visualized by inspecting the variations of streamwise and lateral velocity components. The velocity contours on the weir section help understand the effect of lateral flow on the discharge carrying capacities of the weir gates.

ACKNOWLEDGEMENTS

REFERENCES

Yildiz B, Uijttewaal W (2023) Experimental Analysis of Flow over Rectangular Sharp-Crested Compound Weirs. 40th IAHR World Congress, 21 – 25 August 2023, Vienna, Austria

Qu J, Ramamurthy AS, Tadayon R, Chen Z (2009) Numerical simulation of sharp-crested weir flows. Canadian Journal of Civil Engineering, 36(9), 1530-1534.

Mahtabi G, Arvanaghi H (2018) Experimental and numerical analysis of flow over a rectangular full-width sharp-crested weir. Water Science and Engineering, 11(1), 75-80.

Yildiz B, Uijttewaal W, Bricker J, Mosselman E (2021) Numerical modelling of flow over sharp-crested rectangular contracted weir. The 2nd International Symposium on Water System Operations, Bristol UK

Jiang L, Diao M, Sun H, Ren Y (2018) Numerical modeling of flow over a rectangular broad-crested weir with a sloped upstream face. Water, 10(11), 1663.

Menter F; Esch T (2001) Elements of industrial heat transfer predictions. In Proceedings of the 16th Brazilian Congress of Mechanical Engineering (COBEM), Uberlândia, Brazil, 26–30 November 2001.

Menter FR; Kuntz M; Langtry R (2003) Ten years of industrial experience with the SST turbulence model. Turbul. Heat Mass Transf. 4, 625–632.

Thielicke W, Sonntag R. "Particle Image Velocimetry for MATLAB: Accuracy and Enhanced Algorithms in PIVlab." Journal of Open Research Software, vol. 9, Ubiquity Press, Ltd., 2021, doi:10.5334/jors.334.